TRENDS IN SCIENCES 2025; 22(12): 10543
https://doi.org/10.48048/tis.2025.10543
RESEARCH ARTICLE

Effect of Zn Content on Physicochemical Characteristics, Photocatalytic Activity and Antibacterial Activity of Hydrothermally Synthesized Zn-Doped Hydroxyapatite

Anas Zahra Fauziyyah[1,2], Suresh Sagadevan[3] and Is Fatimah[1,2,*]

[1]Department of Chemistry, Faculty of Mathematics and Natural Sciences, Universitas Islam Indonesia, Kampus Terpadu UII, Yogyakarta 55584, Indonesia
[2]Nanomaterials and Sustainable Chemistry Research Centre, Chemistry Research Laboratory Building, Kampus Terpadu UII, Yogyakarta 55584, Indonesia
[3]Nanotechnology & Catalysis Research Centre, University of Malaya, Kuala Lumpur 50603, Malaysia

([*]Corresponding author's e-mail: isfatimah@uii.ac.id)

Received: 2 May 2025, Revised: 6 May 2025, Accepted: 13 May 2025, Published: 30 August 2025

Abstract

This study explores the effect of zinc (Zn) content on the physicochemical characteristics, photocatalytic activity, and antibacterial activity of hydrothermally synthesized hydroxyapatite (HAp). Zinc doped HAp (Zn-HAp) was synthesized with varying Zn content of 1, 2 and 5 wt%, and characterized using XRD, FTIR, UV-Vis DRS, TEM, and zeta potential analysis. Characterization results showed that Zn was successfully dopped into the HAp structure without forming its own ZnO phase, with a decrease in crystallite size and band gap. Photocatalytic activity test was conducted by degradation of tetracycline (TC) antibiotic using UV light. The results show that Zn-HAp has higher photocatalytic activity than pure HAp, with the highest degradation efficiency of 90.48% obtained at 1Zn-HAp. The photocatalytic activity increased as the band gap decreased, which was facilitated by Zn doping. In addition, antibacterial tests against Escherichia coli and Staphylococcus aureus showed that Zn-HAp had a larger inhibition zone than pure HAp, indicating an increase in antibacterial activity, especially at higher Zn concentrations.

Keywords: Hydroxyapatite, ZnO, Photocatalytic, Antibacterial, Tetracycline

Introduction

The development of industrial activities and medical technologies do not only contribute to the easiness, accessibility and the quality of human life, but also leave some problems related to the quality of environment, drug resistance and health problems such as bacterial infections and cancer disease. The diseases caused by microbial infection and cancer are interrelated and have the potential for significant death risks and are increasing from year to year [1]. Bacterial infections are a major cause of chronic infections and mortality and could promote cancer and increase resistance to anticancer drugs. Antibiotics have been the preferred treatment method for bacterial infections because of their cost-effectiveness and powerful outcomes.

However, antibiotics release in aquatic system is one of the pollution sources need to be resolved and it is an issue to be concerned as an effect of the growing pharmaceutical industries. Tetracycline (TC) is one of the most used antibiotic due to its extensively used not only for human, but also in veterinary and fisheries [2]. Its uncontrolled release from the usages threat to aquatic biodiversity and moreover to its unprecedented use in aquaculture, livestock, and human disease prevention. The accumulation of released TC along the food chain may causes inhibited to microbial system and changes the living organism equilibrium.

Nanotechnology have gets intensive attentions for environmental and medical applications. Within the

scheme, development of smart nanocomposites as photocatalyst for the advanced oxidation process (AOPs) to overcome environmental problems caused by antibiotics and bacterial infections are the important area of research. For medical purposes, some nanocomposites are applied to be host for slow-release drug preparation [3,4]. Among some materials, hydroxyapatite-based nanocomposites are the attractive materials for those varied purposes. Hydroxyapatite (HAp), with chemical formula of $Ca_{10}(PO_4)_6(OH)_2$ (HAp) is a biomaterial widely used in biomedicine as bone and teeth implants, and due to its porosity, it has potency to be modified for environmental remediation applications [5]. The chemical and physical modifications of HAp structure are permittable to enhanced capability for adsorbing organic molecules by increasing hydrophobicity, and to have catalytic activity by attaching metal or metal oxide. In recent years, several studies revealed the feasibility of nanocomposites prepared by the combination of metal/metal oxide with HAp as photocatalyst for organic compounds-contaminated water. Nanocomposites of TiO_2/HAp, Ni-doped HAp, ZrO_2/HAp are some of the nanocomposites exhibited photoactivity for dyes, pharmaceuticals, and toxic organic compounds [6-8] . Photocatalytic activity of the nanocomposite is depending on the activity of incorporated active metal/metal oxide and the physico-chemical characteristics that created.

Previous works highlighted Zn-doped HAp (furthermore called as Zn-HAp) as one of the HAp-based nanocomposites expressed photoactivity and antimicrobial activity against bacteria. However, effect of Zn content as dopant to the nanocomposite to these activities was not intensively studied yet. The photoactivity of Zn-doped Hydroxyapatite is related to the activity of ZnO as a photocatalyst in the degradation of dyes and antibiotics in previous studies. Photoactivity is influenced by band gap energy which is related to its morphology [9]. Using previous investigations highlighted the effectiveness of hydrothermal synthesis method [10,11] considering these potential roles of Zn-HAp, this work aimed to explore the characteristics of Zn-HAp as photocatalyst and antibacterial agent. Study considers on the effect of Zn content to the physicochemical characteristics and the activities of the materials.

Materials and methods

Materials

Chemicals used in this research consist of CaO, $(NH_4)_2HPO_4$, $ZnCl_2.2H_2O$, NaOH, sodium citrate were purchased from Merck-Millipore (Darmstadt, Germany), tetracycline was produced by Sigma-Aldrich. All chemicals used were of analytical reagent grade and were used without any further purification

Synthesis of Zn-HAp

Zinc-doped hydroxyapatite (Zn-HAp) was synthesized with varied Zn content; 1, 2 and 5 %wt, therefore the resulted samples denoted as 1Zn-HAp, 2Zn-HAp and 5Zn-HAp, respectively. The synthesis process consists of 2 steps: Co-precipitation and hydrothermal treatment. The precursors consist of CaO, and zinc acetate were mixed in a deionized water, and furthermore ($(NH_4)H_2PO_4$) was slowly added into the solution to get [(Ca+Zn)/P] molar ratio of 1.67. The mixture was vigorously stirred and CTAB 2% was added to prevent rapid aggregation. Finally, sodium citrate was then added as a buffer to fix the pH = 10 for precipitation. The slurries from varied Zn content obtained from these steps were then transferred into aTeflon-lined autoclave for a hydrothermal process at 150 °C overnight. The resulting slurry was dried at 120 °C. Pristine HAp was prepared with similar procedure on (Ca/P) molar ratio of 1.67.

Materials characterization

X-ray diffraction (XRD) analysis to the samples was performed on a Shimadzu X6000 instrument from 5° to 80° at the rate of 0.2°/min with Ni-filtered CuKα radiation (λ= 1.54 Å) at 40 kV and 30 mA current. FE-SEM analysis was recorded on a HITACHI SEM8010 (Japan) instrument operated at 30 kV in the back-scattered electron detector and secondary electron detector modes. Transmission electron microscopy (TEM) analysis was performed using a JEM 2010 instrument. Surface analysis using X-ray Photoelectron Spectroscopy (XPS) was performed on an ULVAC spectrometer, Quentera SXM (Japan).

Photocatalytic activity examination

Photocatalytic activity of the prepared samples was examined on TC photocatalytic degradation using a

water-jacketed batch photoreactor equipped with UV lamp (300 nm, 20 watt, 31.22 MW/cm^2). For each examination, about 0.2 g of the photocatalyst samples were added into 250 mL of TC solution (20 mg/L) for exposed by lamp along the stirring. Sampling was taken at 0, 15, 30, 45, 60, 90 and 120 min, and the TC concentration was determined based on UV-Visible spectrophotometric analysis on the wavelength of 356 nm. A Hitachi U-2080 UV-Visible spectrophotometer was employed for analysis. Degradation efficiency (RE) (%) was calculated using the following Eq. (1):

$$\mathrm{RE}(\%) = \frac{C_0 - C_t}{C_0} \times 100 \quad (1)$$

where C_0 and C_t are the concentrations of TC at the initial and time of sampling *t*, which the concentration of TC.

Antibacterial assay

Antibacterial assay of the prepared samples towards *E. coli* and *S. aureus* bacteria was conducted using agar well diffusion method. The samples powders were dispersed in demineralized water to get the concentration of 5 mg/5 mL followed by immersing onto a 6 mm filter disc. The obtained discs were placed on the bacteria cultures that were prepared by sub-cultured and incubation at 37 °C for 24 h. The microbial growth was monitored overnight, and then the clear zone representing the bacterial inhibition was measured.

Figure 1 provides a schematic procedure of synthesis, characterization, photoactivity test and antibacterial assay of the samples.

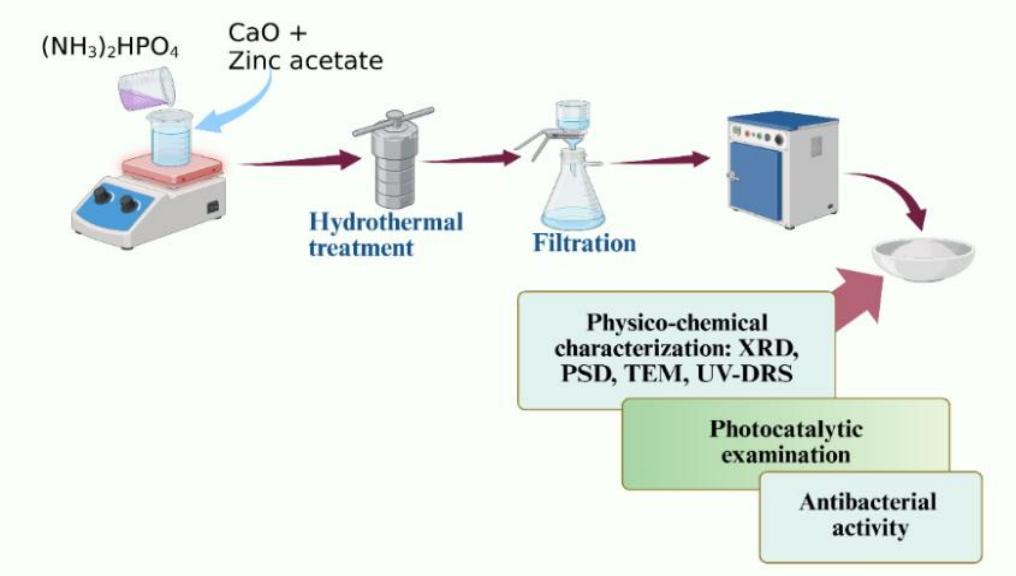

Figure 1 Schematic representation of synthesis, characterization and antibacterial activity of prepared materials.

Results and discussion

XRD analysis

XRD characterization is used to determine the crystal structure and the crystallite size of the materials. The obtained XRD results are presented in **Figure 2**.

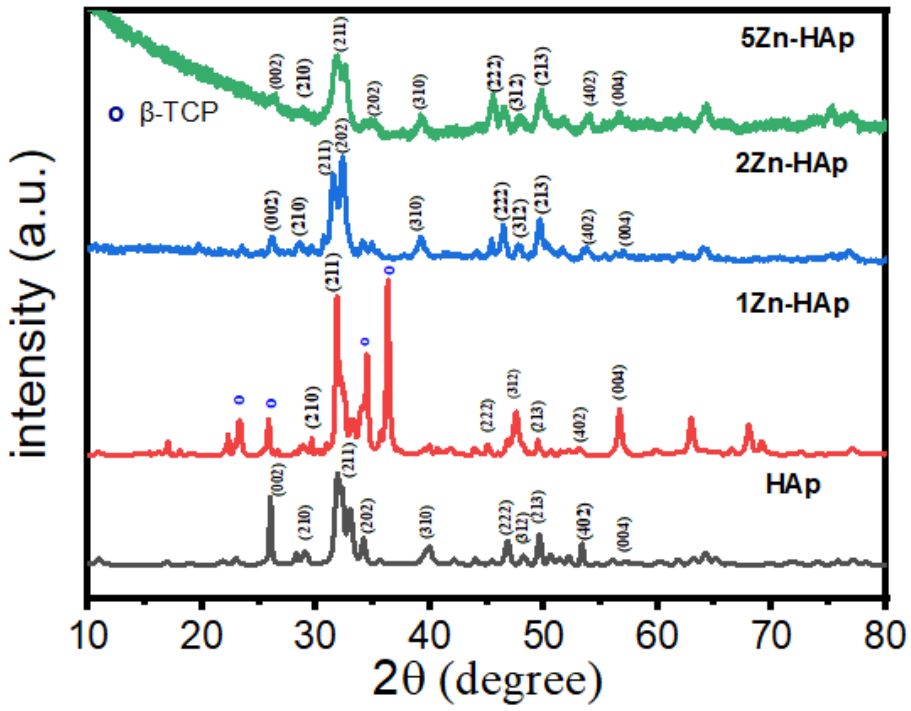

Figure 2 XRD patterns of prepared samples.

It is seen that all samples show the peaks at 26.12°, 28.64°, 31.54°, 32.30°, 39.18°, 46.42°, 47.78°, 49.66°, 53.80° and 56.98° that are associated to the reflections of (002), (210), (211), (202), (310), (222), (312), (213), (402) and (004) planes of HAp refered to JCPDS NO. 09-0432 [12]. There are no peaks associated to the presence of ZnO identified in all samples, suggesting that Zn is incorporated into the HAp structure and does not form a separate oxide phase [13]. It was found that all Zn-HAp samples exhibited a slight shift compared to the HAp peaks while maintaining the dominant HAp phase. The shift of X-ray diffraction peaks to lower angles is likely due to the incorporation of Zn into the HAp lattice, which alters the unit cell dimensions or induces lattice distortion due to the ionic size difference between Zn^{2+} and Ca^{2+}. The Zn doping not only causes a slight increase in lattice parameters but also enhances the crystallinity of HAp, as indicated by the higher degree of crystallinity values. The incorporation of Zn into the HAp structure not only accelerates the formation of a more ordered crystalline phase but also results in an increase in crystallite size [14].

Different to other Zn-HAp samples, 1Zn-HAp exhibits some additional peaks 23.37°; 25.88° ; 34.43° ; and 36.29° that are corresponding to the (101), (214), (0210), and (220) planes of β-TCP referred to JCPDS No. 9-0169 [15]. This indicates that during synthesis, the calcium and phosphate precursors were not fully incorporated into the HAp structure. This is due to the doping of Zn into HAp, which replaces Ca positions, leading to Ca deficiency in Zn-HAp. Consequently, the substitution of Ca ions with Zn ions results in the formation of a new phase, β-TCP [15].

Based on all identified peaks, the particle size of HAp in each sample were determined using the Scherrer equation (Eq. (2)):

$$D = \frac{K\lambda}{\beta \cos\theta} \quad (2)$$

with D is the average crystallite size (diameter), α is the wavelength of X-rays (1.54 nm), θ is the diffraction angle, and β represents the Full Width at Half Maximum (FWHM). The calculated crystallite size results are presented in **Table 1**.

Table 1 Calculations on crystallite size of Zn-HAp samples.

2θ (degree)	HAp		1Zn-HAp		2Zn-HAp		5Zn-HAp	
	FWHM	Crystal size (nm)	FWHM	Crystal size (nm)	FWHM	Crystal size (nm)	FWHM	Crystal size (nm)
26.25°	0.2415	32.07	0.193	40.14	0.4410	17.55	17.230	0.45
29.6°	0.1517	6.68	0.131	58.66	0.7689	10.02	5.072	1.52
31.90°	0.6461	11.82	0.254	30.10	0.6000	12.75	1.831	4.17
34.95°	1.6348	4.64	0.260	29.19	0.4826	15.82	4.671	1.62
39.92°	0.7941	9.40	0.245	30.81	0.6712	11.15	9.184	0.81
46.86°	0.4686	15.56	0.366	20.04	0.4550	16.05	0.455	16.03
48.82°	0.4028	18.00	0.505	14.39	0.4510	16.11	18.402	0.39
49.74°	0.3858	18.70	0.240	30.05	0.5394	13.37	82.176	0.08
53.86°	0.2783	25.51	0.190	37.39	0.6841	10.36	0.377	18.80
56.98°	0.3705	18.93	0.282	24.80	0.3705	18.85	27.135	0.26
Average = 16.13 nm			Average	= 31.56 nm	Average	= 14.2 nm	Average	= 4.41 nm

Based on the results presented in **Table 1**, the average crystallite sizes of HAp, 1Zn-HAp, 2Zn-HAp, and 5Zn-HAp were determined to be 16.13, 31.56, 14.02 and 4.41 nm, respectively. These findings indicate that the analyzed particles fall within the nanoparticle range. The observed decrease in crystallite size is consistent with the literature by Ofudje [14] which attributes this trend to the increasing concentration of metal dopants, leading to peak broadening. Additionally, the smaller ionic radius of Zn^{2+} contributes to the structural contraction of HAp, further reducing crystallite size.

FTIR technique is an effective method for analyzing the composition of material components. FTIR is used to identify the functional groups present in the synthesized material, allowing for the determination of the success of HAp synthesis. The FTIR spectrum of the Zn-HAp material is presented in **Figure 3**.

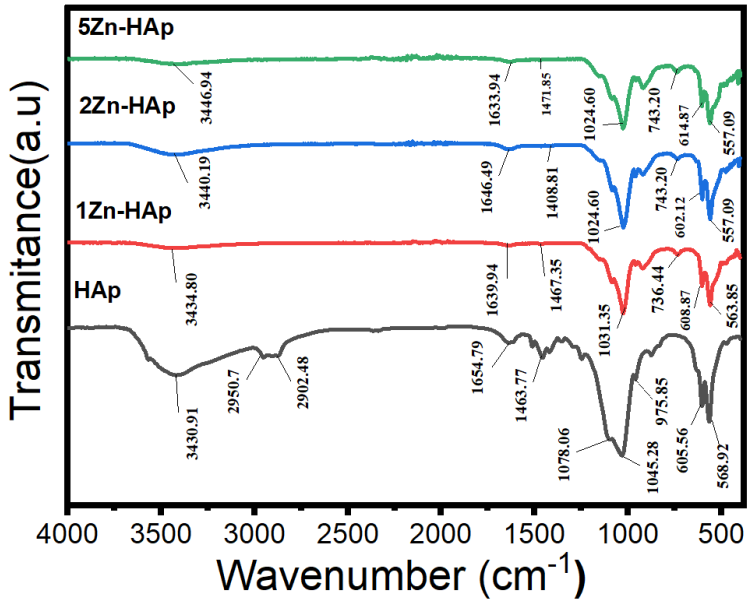

Figure 3 FTIR spectra of the prepares samples.

The FTIR absorption spectrum of HAp nanoparticles with variations of 1Zn-HAp, 2Zn-HAp, and 5Zn-HAp, synthesized and analyzed in the frequency range of 4,000 to 500 cm^{-1}, is shown in the figure. All bands in the spectrum correspond well with the previously reported IR data for HAp. The sharp absorption peaks at around 1,024.60 - 1,045.28 cm^{-1} in all samples are associated to the stretching mode of phosphate groups (PO_4^{3-}) [17,18]. Additionally, a broad stretching band in HAp appears at 1,463.77 cm^{-1}. which is associated with carbonate group (CO_3^{2-}) [19]. The peak at 1,463.77 cm^{-1} which appeared in HAp is not observed in Zn-doped HAp samples, suggesting that the incorporation of Zn^{2+} ions into the apatite lattice replace calcium ion in HAp structure. This observation aligns with the XRD results, which indicate a decrease in apatite crystallinity as the Zn concentration increases.

The absorptions at around 1,654.79 cm^{-1} for all sample are associated with the absorbed water molecules [20], which also correlated to the weak band observed around 3,430 cm^{-1} in and at around 3,434.80 cm^{-1}. These bands primarily correspond to the O–H stretching vibrations within the crystal lattice of hydroxyapatite [21]. This band is not observed in the HAp lattice and is attributed to the liberation mode of OH groups, which is less pronounced in biological apatite. The FTIR spectra of the analysed samples exhibit peak broadening and smoothing as the zinc concentration increases. This behaviour may indicates a reduced crystallinity along with increasing zinc content, and it is consistence with previous experimental findings by Ren *et al.* [21] which reported that crystal size and the intensity decrease as Zn concentration increases.

UV-visible DRS

The band gap energy of a material is determined using diffuse reflectance UV-DRS spectroscopy, and the Tauc's plots are provided in **Figure 4**. It is observed that the band gap energy values are 4.63, 3.56, 3.58 and 3.62 eV for HAp, 1Zn-HAp, 2Zn-HAp, and 5Zn-HAp, respectively. The data suggests that zinc doping reduces the band gap energy of HAp, attributed to a blue shift caused by a shift toward shorter wavelengths. The larger the band gap energy, the more energy is required to excite electrons from the valence band to the conduction band. The band gap is determined by electron movement from the valence band to the conduction band, where increased absorbance leads to higher energy absorption by the material, resulting in a decrease in the measured band gap energy [22].

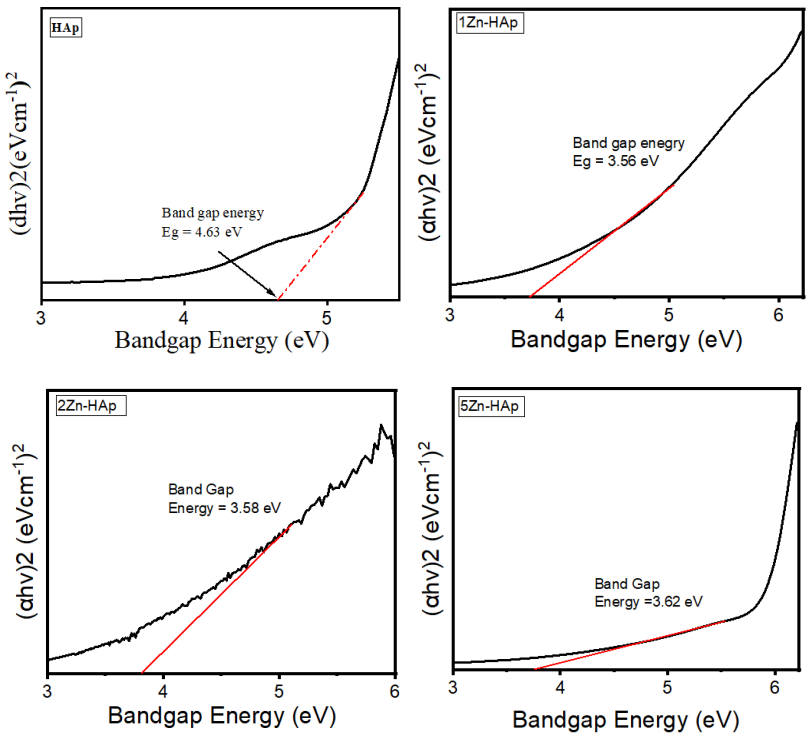

Figure 4 Tauc's plots of prepared materials.

Particle's size distribution and zeta potential measurements of the samples

Particle Size Distribution (PSD)and zeta potential analyses were performed used to determine the average nanoparticle size and the electrical properties if particle's surface of the materials. **Figure 5** illustrates the particle's size distribution of HAp, 1Zn-HAp, 2Zn-HAp, and 5Zn-HAp, which were measured to be 39.84, 39.8, 39.19 and 36.33 nm, respectively, indicating that these materials fall within the nanoparticle size range. The results from PSD analysis is in line with the results from TEM measurement provided in **Figure 6**. Based on previous research, particle size is related to band gap energy where the smaller the particle size will produce a higher band gap energy which increases the photoactivity of the material. lower particle size results in a larger surface area that facilitates interaction with bacterial cells. Thus, creating antibacterial activity [23,24].

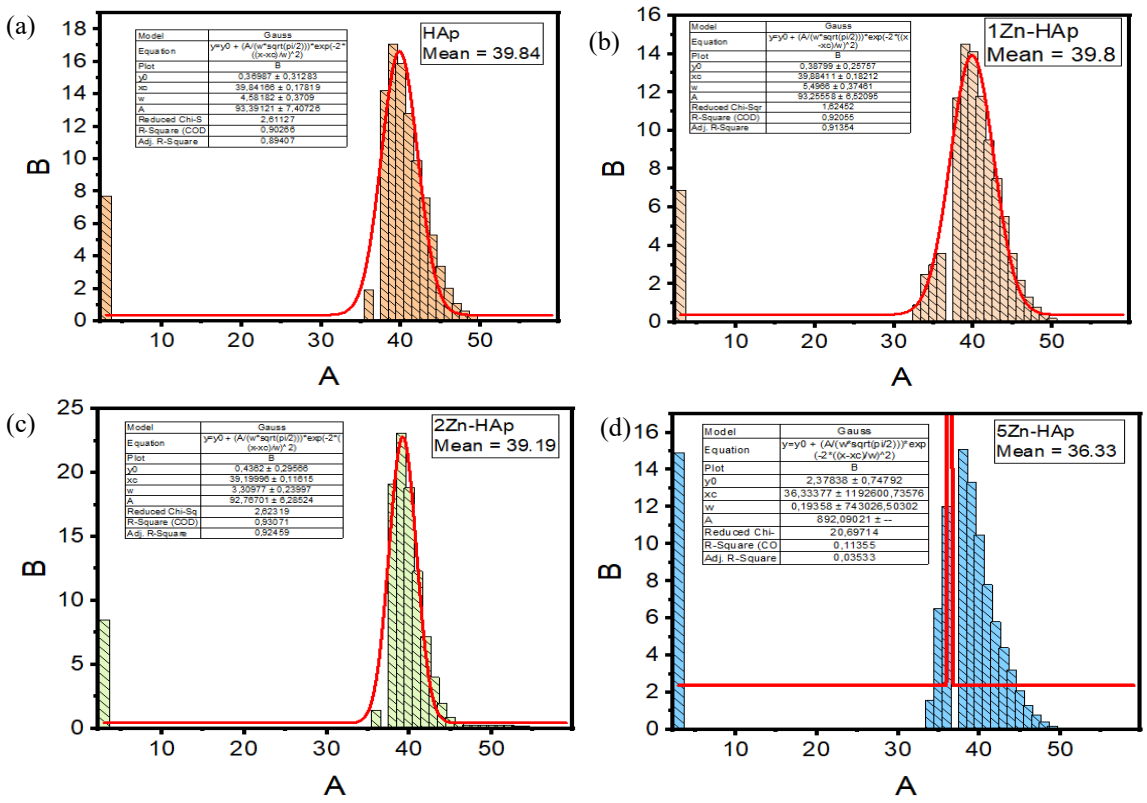

Figure 5 Particle's size distribution of the prepared sample.

The HAp and 5Zn-HAp shows rod-like particles similar 3 to the appearance reported by previous works [25,26]. Particle size distribution measurement to the exhibited particles gives the mean particle size of 31.3 and 23.8 nm, for HAp and 5Zn-HAp, respectively.

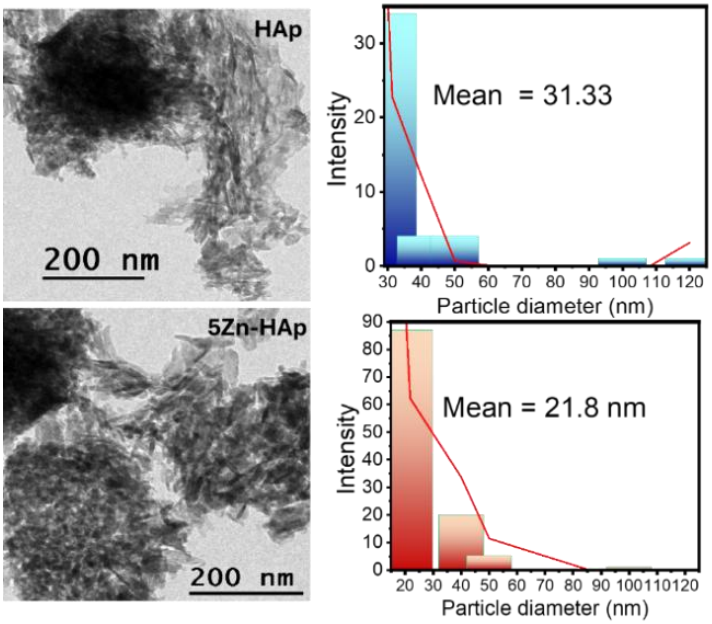

Figure 6 TEM images of HAp and 5Zn-Hap.

The zeta potential (**Figure 7**) measurement gives the values of –13.4, –33.3, –29.5 and –28.4 mV for HAp, 1Zn-HAp, 2Zn-HAp, and 5Zn-HAp, respectively. A negative zeta potential indicates that the dispersed particles in the suspension carry a negative charge. Based on previous research, the presence of smaller metal ion changes the zeta potential via the change of their bonding with the negative charge of phosphate (PO_4^{3-}) and hydroxyl (^{-}OH) dominates over Ca^{2+} ions. The higher-level zeta potential of Zn-HAp compared to HAp is related to the capability of surface to inhibit the aggregation. Furthermore, for their interaction with bacteria, more negatively charged of the surface leads the surface easier to bind with protein [27,28]. The values are also comparable and in the range of that of the nanocomposite formed by the combination of metal and hydroxyapatite [29].

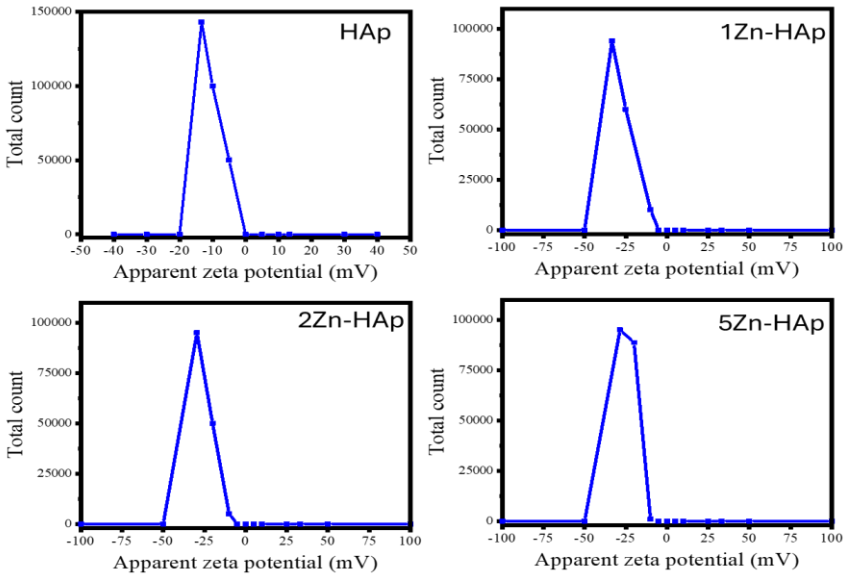

Figure 7 Zeta potential measurement of the prepared samples.

Photocatalytic activity test

Kinetics of TC photocatalytic degradation using the prepared materials compared to the adsorption process is depicted by the kinetics plots in **Figures 8(a)** and **8(c)**. As can be seen from the plots that all Zn-HAp samples show the higher photocatalytic activity compared to HAp as shown by the faster reduced concentration observed at all times of treatment. The Based on the obtained DE values at 120 min, the photocatalytic activity of the samples is in following order: 1Zn-HAp > 5Zn-HAp > 2Zn-HAp > HAp. This order is different from the order obtained by adsorption process as HAp gave highest adsorption capability and the order is as follow: HAp > 2Zn-HAp> 5Zn-HAp > 1Zn-HAp. The phenomenon of the higher adsorption efficiency over HAp compared to other samples referred to the specific surface area of solid sample provided by HAp and the less negative zeta potential of HAp compared to Zn-HAp samples. The higher negative values of Zn-HAp samples represent the more anionic groups on the surface that may affect to the repulsive interaction among HAp-TC. From previous investigation on TC adsorption by TiO_2 nanoparticles, it was found that the increasing of zeta potential of the nanoparticles leading to a larger electrostatic repulsion force that prevented the further aggregation [29,30]. The kinetics study for photocatalytic experimental data, process revealed that the reaction obeys pseudo-1st order kinetics with following equation (Eq. (3)):

$$\ln C_t = \ln C_0 - kt \quad (3)$$

With C_t and C_0 are TC concentration at time of t and at initial, k is kinetics constant of the reaction, and t is time of the reaction. Meanwhile, from the adsorption experimental data, intraparticle diffusion (IPD) kinetic model equation was applied referred to following equation.

The parameters obtained from the kinetics calculations are provided in **Table**

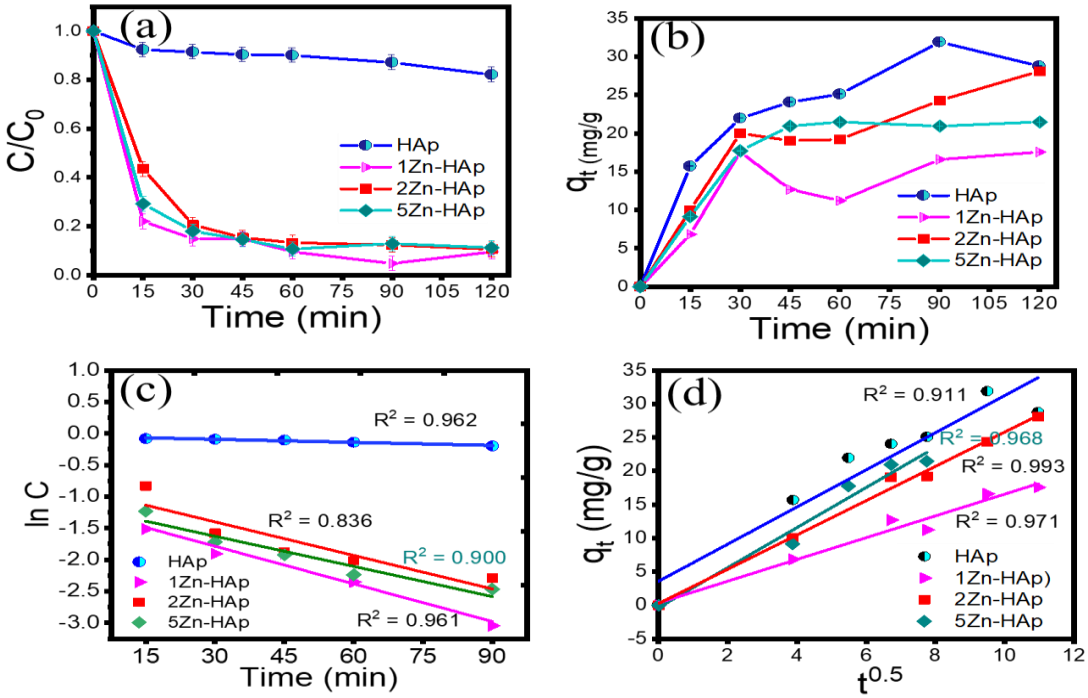

Figure 8 (a) Kinetics plot of TC removal by photocatalytic degradation, (b) Kinetics plot of TC removal by adsorptiom, (c) 1st-order kinetics plot of TC photocatalytic degradation, (d) IPD kinetics plot of TC removal by adsorption.

Table 1 Kinetics parameters of photocatalytic degradation and adsorption of TC using prepared materials.

Photocatalytic degradation				
Sample	**Kinetics equation**	k/k_i	R^2	**DE**
HAp	$lnC_t = 1.61\times10^{-3}t - 4.44\times10^{-2}$	1.61×10^{-3}	0.962	17.89
1Zn-HAp	$lnC_t = 1.98\times10^{-2}t - 1.19$	1.98×10^{-2}	0.961	90.48
2Zn-HAp	$lnC_t = 1.77\times10^{-2}t - 8.69\times10^{-1}$	1.77×10^{-2}	0.836	89.41
5Zn-HAp	$lnC_t = 1.59\times10^{-2}t - 1.15$	1.59×10^{-2}	0.900	88.76
Adsorption				
Sample	**Adsorption kinetics equation**		R^2	q_t **(mg/g)**
HAp	$q_t = 2.77t + 3.57$	2.77	0.911	35.94
1Zn-HAp	$q_t = 1.62t + 0.33$	1.62	0.971	21.95
2Zn-HAp	$q_t = 2.56t + 0.27$	2.56	0.993	35.11
5Zn-HAp	$q_t = 2.17t + 2.56$	2.17	0.968	26.84

From the calculated adsorption capacity measured for TC concentration of 10 mg/L, the values obtained in this work is comparable to similar works, for example the q_e of 32 mg/g observed by HAp Kanmaz and Demircivi [31] and the q_e of HAp and ZnO-HAp samples ranging from 5 - 35 mg/g [32]. In addition, the photocatalytic activity of all Zn-HAp samples is also comparable to ZnO-HAp samples prepared by previous researchers in which TC removal of 85.5% was achieved on 20 %wt. of Zn in the ZnO-HAp nanocomposite under visible lamp [22]. Meanwhile, the photocatalytic of HAp is similar to the photoactivity of HAp in similar works [33,34]. The higher photocatalytic activity is exhibited by Zn-HAp samples compared to Zr-doped HAp as in the degradation process, no additional oxidant such as H_2O_2 is consumed with similar DE values [34].

Antibacterial assay

Antibacterial assay of the samples was performed using the disk diffusion method, which is the most employed technique for this type of evaluation. The inhibition zones or clear zones were measured as the test parameter, indicating the antibacterial efficacy of the material. The disk diffusion method was chosen due to its simplicity and the minimal equipment required. The antibacterial medium used in this study includes *Nutrient Broth* (NB) for bacterial growth on the material and *Mueller-Hinton Agar* (MHA) as the agar medium in petri dishes, providing ample nutrients essential for bacterial inhibition. The tested bacterial strains included both Gram-positive and Gram-negative bacteria of *S. aureus* and *E. coli*, respectively.

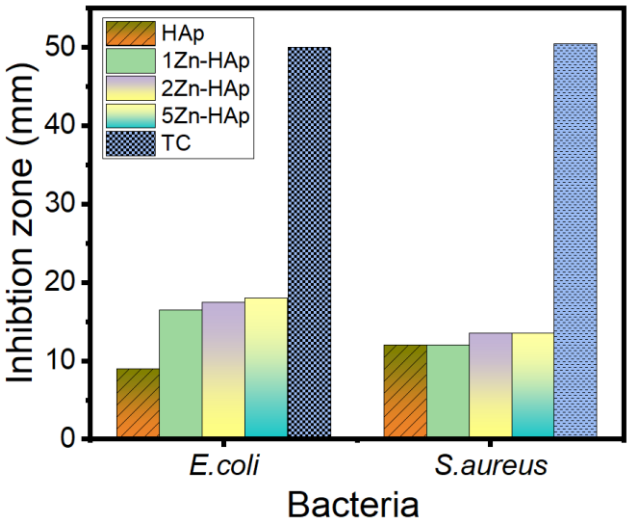

Figure 9 Measured inhibition zone from antibacterial assay of samples against *E. coli* and *S. aureus*.

The results provided in **Figure 9** indicate that the Zn-HAp samples exhibited higher antibacterial activity compared to the HAp sample. For antibacterial assay against *E. coli*, the measured inhibition zone of HAp, 1Zn-HAp, 2Zn-HAp, and 5Zn-HAp are 9, 16.5, 17.5 and 18 mm, respectively. Meanwhile, towards *S.aureus*, the inhibition zones are 12 mm for both HAp and 1Zn-HAp, and 13.5 mm for both 2Zn-HAp and 5Zn-HAp. Conclusively, the stronger antibacterial effect is achieved at the higher Zn amount in the nanocomposite can be attributed to the higher potency of the sample in releasing Zn ions to be introduced to the cell wall [35,36]. The higher Zn content increased the inhibition zone towards *E. coli*, which is in a similar trend with previous work [37]. The increased antibacterial activity is related to the physicochemical characteristics of particle size and zeta potential that are significantly observed as the function of zinc content. The less particle size facilitates the diffusion of Zn-HAp particles with cell walls and obstruction of metabolic processes of bacteria [38]. In addition, referred to previous investigation, the higher Zn content in Zn-HAp accelerated the rate of Zn^{2+} releasing [39].

According to the inhibition zone, the data are laid on strong antibacterial activity, and these are comparable to were reported by similar nanocomposites as listed in **Table 2**. The measured inhibition zone value of the pristine HAp reflected the antibacterial activity of the sample without any dopant, and even more it is the same with the activity of 1Zn-HAp towards *S.aureus*. This is due to the capability of the sample to release Ca^{2+} to interrupt the cell wall of bacteria [40].

Table 2 Comparison of the antibacterial activity of metal-doped hydroxyapatite.

Material	Results	Reference
Zn-HAp	The inhibition zones of material against *E. coli* and *S. Aureus* after 4 h of incubation were 0.25 and 6.65 mm, respectively.	[41]
HAp	The synthesized n-HAp exhibited an inhibition zone of 5 mm against *S. aureus*.	[42]
Zn-HAp	The obtained Zn-HAp demonstrated the inhibition zones of 16 and 12 mm against *E. coli* and *S. Aureus*, respectively.	[43]
Zn-HAp	The antibacterial examination of the sample towards *E. coli* and *S. aureus* gave inhibition zones of 10 and 9.3 mm, respectively.	[44]
Ag-HAp	The highest inhibition zone at an Ag-HAp concentration of 5% was recorded at 19.7 mm against *E. coli* and 13.8 mm against *S. aureus*.	[45]
Zn-HAp	The material exhibited a strong antimicrobial activity against *E. coli* and *S. aureus* as shown by the inhibition zone of 22.7 and 8 mm, respectively.	[35]

The remarkable results that have been observed from this work are that the physicochemical characteristics Zn-HAp are governed by the zinc content in the nanocomposite. The higher Zn content ranging at 1 - 5 %wt. effects on the decreasing particle size and band gap energy that are significant parameters for photocatalytic activity enhancement. In other side, the increased antibacterial activity along with the increased Zn content is related to smaller particle size and more negative zeta potential that determine the faster releasing Zn^{2+} ion and more intensive interaction of the particles with bacterial cell wall. The data ensures the importance of optimizing physicochemical character and potential applicability of Zn-HAp nanocomposites for environmental and medical applications.

Conclusions

Hydrothermal synthesized zinc-doped hydroxyapatite with a varied zinc content has been successfully conducted. The physicochemical characterization revealed that zinc dopant is neither influences the hydroxyapatite structure significantly, nor created ZnO phase, indicating the doped structure. At the Zn content of 1 %wt., the Zn doping affected to the formation of β-tricalcium phosphate. The insertion of Zn in HAp structure reduced the band gap energy and particle's size distribution. This effect was confirmed by TEM measurement revealing the less particle size of Zn-HAp samples compared to HAp. The Zn-HAp exhibited lower band gap energy that contribute to enhance photocatalytic activity. The photoactivity was expressed by the capability for tetracycline degradation with the highest DE of 90.48 % obtained using 1Zn-HAp. The enhanced antibacterial activity was also expressed by Zn-HAp samples compared to HAp.

Acknowledgements

Authors thank Kementrian Riset DIKTI for Penelitian Tesis Magister 2024.

Declaration of Generative AI in Scientific Writing

There is no AI utilized in research and manuscript writing

CRediT author statement

Anas Zahra Fauziyyah: Data curation, Formal Analysis, Sample preparation. **Suresh Sagadevan**: Instrumental analysis, Validation, Methodology, Writing–review and editing. **Is Fatimah**: Conceptualization, Methodology, Validation, Methodology, Writing–original draft

References

[1] H Alioui, O Bouras and JC Bollinger. Toward an efficient antibacterial agent: Zn- and Mg-doped hydroxyapatite nanopowders. *Journal of Environmental Science and Health - Part A Toxic/Hazardous Substances and Environmental Engineering* 2019; **54(4)**, 315-327.

[2] K Yusuf, V Sampath and S Umar. Bacterial infections and cancer: Exploring this association and its implications for cancer patients. *International Journal of Molecular Sciences* 2023; **24(4)**, 3110.

[3] F Ahmad, D Zhu and J Sun. Environmental fate of tetracycline antibiotics: Degradation pathway mechanisms, challenges, and perspectives. *Environmental Sciences Europe* 2021; **33(1)**, 64.

[4] J Wang and R Zhuan. Degradation of antibiotics by advanced oxidation processes: An overview. *In Science of the Total Environment* 2020; **701**, 135023.

[5] J Ma, Y Chen, G Zhou, H Ge and H Liu. Recent advances in photocatalytic degradation of tetracycline antibiotics. *Catalysts* 2024; **14(11)**, 762.

[6] S Mondal, S Park, J Choi, TTH Vu, VHM Doan, TT Vo, B Lee and J Oh. Hydroxyapatite: A journey from biomaterials to advanced functional materials. *Advances in Colloid and Interface Science* 2023; **321**, 103013.

[7] TCN Nicácio, MAM Castro, MCN Melo, TA Silva, MD Teodoro, MRD Bomio and FV Motta. Zn and Ni doped hydroxyapatite: Study of the influence of the type of energy source on the photocatalytic activity and antimicrobial properties. *Ceramics International* 2024; **50(15)**, 27540-27552.

[8] MB Febrian, I Mahendra, A Kurniawan, Y Setiadi, THA Wibawa, R Lesmana and DG Syarif.

Zirconium doped hydroxyapatite nanoparticle as a potential design for lung cancer therapy. *Ceramics International* 2021; **47(19)**, 27890-27897.

[9] I Fatimah, H Hidayat, PW Citradewi, M Tamyiz, R Doong and S Sagadevan. Hydrothermally synthesized titanium/hydroxyapatite as photoactive and antibacterial biomaterial. *Heliyon* 2023; **9(3)**, e14434.

[10] P Porrawatkul, R Pimsen, A Kuyyogsuy, P Rattanaburi and P Nuengmatcha. Morphology-dependent photocatalytic performance of ZnO nanostructures in organic dye and antibiotic degradation. *International Journal of Environmental Science and Technology* 2024; **21(2)**, 7397-7414.

[11] P Szterner and M Biernat. The synthesis of hydroxyapatite by hydrothermal process with calcium lactate pentahydrate: The effect of reagent concentrations, pH, temperature, and pressure. *Bioinorganic Chemistry and Applications* 2022; **2022**, 3481677.

[12] M Andrean, M Castro, T Portela, G Sousa, M Moizinho, J Hilton, G Rangel, S Filgueiras, J Manuel and R Mercury. Synthesis of hydroxyapatite by hydrothermal and microwave irradiation methods from biogenic calcium source varying pH and synthesis time. *Boletín de la Sociedad Española de Cerámica y Vidrio* 2020; **61(1)**, 35-41.

[13] J Liu, X Ye, H Wang, M Zhu, B Wang and H Yan. The influence of pH and temperature on the morphology of hydroxyapatite synthesized by hydrothermal method. *Ceramics International* 2003; **29(6)**, 629-633.

[14] EA Ofudje, AI Adeogun, MA Idowu and SO Kareem. Synthesis and characterization of Zn-Doped hydroxyapatite: Scaffold application, antibacterial and bioactivity studies. *Heliyon* 2019; **5(5)**, e01716.

[15] S Kato, S Kagawa, K Saito and M Ogasawara. Incorporation and deposition behaviors of Cu and Ni ions into hydroxyapatite channels by heat treatment. *Journal of Physics and Chemistry of Solids* 2023; **177**, 111287.

[16] M Irfan, SN Sultana, B Venkateswarlu, M Jagannatham, R Dumpala and BR Sunil. Zinc-substituted hydroxyapatite: Synthesis, structural analysis, and antimicrobial behavior. *Transactions of the Indian Institute of Metals* 2021; **74(9)**, 2335-2344.

[17] E Andrew, A Idowu, M Abidemi and S Olateju. Heliyon synthesis and characterization of zn-doped hydroxyapatite: Scaffold application , antibacterial and bioactivity studies. *Heliyon* 2019; **5**, e01716.

[18] GS Kumar, A Thamizhavel, Y Yokogawa, SN Kalkura and EK Girija. Synthesis, characterization and *in vitro* studies of zinc and carbonate co-substituted nano-hydroxyapatite for biomedical applications. *Materials Chemistry and Physics* 2012; **134(2-3)**, 1127-1135.

[19] M Hamza, Q Kanwal, Z Ali, S Zargar, AH Alshammari, TA Wani, M Rizwan, K Rohm and MA Mushtaq. Exploring the molecular biology of zinc-doped hydroxyapatite nanocomposites as fillers for dental materials: A self-defensive approach targeting bacterial DNA. *Materials Research Express* 2024; **11(9)**, 095401.

[20] M Iafisco, JG Morales, MA Hernández-Hernández, JM García-Ruiz and N Roveri. Biomimetic carbonate-hydroxyapatite nanocrystals prepared by vapor diffusion. *Advanced Engineering Materials* 2010; **12(7)**, B218-B223.

[21] J Jia, H Zhou, J Wei, X Jiang, H Hua, F Chen, S Wei, JW Shin and C Liu. Development of magnesium calcium phosphate biocement for bone regeneration. *Journal of the Royal Society Interface* 2010; **7(49)**, 1171-1180.

[22] F Ren, RvXin, X Ge and Y Leng. Characterization and structural analysis of zinc-substituted hydroxyapatites. *Acta Biomaterialia* 2009; **5(8)**, 3141-3149.

[23] Y Chen, R Zou and Q Wu. Facile synthesis of hollow ZnO/HAp microsphere photocatalysts for efficient removal of tetracycline under full light irradiation. *Inorganic Chemistry Communications* 2025; **174**, 114084.

[24] I El-Habib, H Maatouk, A Lemarchand, S Dine, A Roynette, C Mielcarek, M Traoré and R Azouani. Antibacterial size effect of ZnO nanoparticles and their role as additives in emulsion waterborne paint. *Journal of Functional Biomaterials* 2024; **15(7)**, 195.

[25] N Babayevska, Ł Przysiecka, I Iatsunskyi, G Nowaczyk, M Jarek, E Janiszewska and S Jurga. ZnO size and shape effect on antibacterial activity and cytotoxicity profile. *Scientific Reports* 2022; **12(1)**, 8148.

[26] V Kalaiselvi, R Mathammal and P Anitha. Sol-gel mediated synthesis of pure hydroxyapatite at different temperatures and silver substituted hydroxyapatite for biomedical applications. *Journal of Biotechnology & Biomaterials* 2017; **07(4)**, 1-6.

[27] APS Prasanna and GD Venkatasubbu. Sustained Release of amoxicillin from hydroxyapatite nanocomposite for bone infections. *Progress in Biomaterials* 2018; **7**, 289-296.

[28] X Jiang, Y Zhao, C Wang, R Sun and Y Tang. Effects of physico-chemical properties of ions-doped hydroxyapatite on adsorption and release performance of doxorubicin as a model anticancer drug. *Materials Chemistry and Physics* 2022; **276**, 125440.

[29] GT El-Bassyouni, SH Kenawy, AAAE Aty, EMA Hamzawy and GM Turky. Influence of ZnO doped into hydroxyapatite: Structural, electrical, biocompatibility, and antimicrobial assessment. *Journal of Molecular Structure* 2022; **1268(1)**, 133700.

[30] MS Elsayed, IA Ahmed, DMD Bader and AF Hassan. Green synthesis of nano zinc oxide/nanohydroxyapatite composites using date palm pits extract and eggshells: Adsorption and photocatalytic degradation of methylene blue. *Nanomaterials* 2022; **12(1)**, 49.

[31] N Qi, P Wang, C Wang and Y Ao. Effect of a typical antibiotic (tetracycline) on the aggregation of TiO2 nanoparticles in an aquatic environment. *Journal of Hazardous Materials* 2018; **341**, 187-197.

[32] N Kanmaz and P Demircivi. Adsorption of tetracycline using one-pot synthesis zirconium metal-organic framework (UiO-66) decorated hydroxyapatite. *Journal of Molecular Liquids* 2024; **397**, 124171.

[33] C Oliveira, ALMD Oliveira, L Chantelle, R Landers, S Medina-Carrasco, MDM Orta, ECS Filho and MG Fonseca. Zinc (II) modified hydroxyapatites for tetracycline removal: Zn (II) doping or ZnO deposition and their influence in the adsorption. *Polyhedron* 2021; **194**, 114879.

[34] I Fatimah, R Audita, G Purwiandono, H Hidayat, S Sagadevan, WC Oh and R Doong. In-situ synthesis of hydroxyapatite-supported Ag_3PO_4 using cockle (Anadara granosa) shell as photocatalyst in rhodamine B photodegradation and antibacterial agent. *Case Studies in Chemical and Environmental Engineering* 2024; **10**, 100797.

[35] I Fatimah, G Purwiandono, GD Ramanda, N Nurlaela, H Hidayat, S Sagadevan and WC Oh. Zr-doped hydroxyapatite nanorods from cockle shell and study on photocatalyst activity and cytotoxicity. *Inorganic Chemistry Communications* 2024; **165**, 112559.

[36] A Bhattacharjee, A Gupta, M Verma, PA Murugan, P Sengupta, S Matheshwaran, I Manna and K Balani. Site-specific antibacterial efficacy and cyto/hemo-compatibility of zinc substituted hydroxyapatite. *Ceramics International* 2019; **45(9)**, 12225-12233.

[37] ML Habib, SA Disha, MS Hossain, MN Uddin and S Ahmed. Enhancement of antimicrobial properties by metals doping in nano-crystalline hydroxyapatite for efficient biomedical applications. *Heliyon* 2024; **10(1)**, e23845.

[38] JR Guerra-López, AE Bianchi, MA Ramos, M Ubertino, V Ferraresi-Curotto, JA Güida, K Barbaro, AA Zhukova, VY Grigorieva, JV Rau and GA Echeverría. Preparation of Zinc-doped hydroxyapatite ceramics and evaluation of biocompatibility and antibacterial activity. *Journal of Functional Biomaterials* 2025; **16(3)**, 88.

[39] A Anwar, A Sadiqa, A Intisar, AU Rashid, T Razaq, SA Aldossari, MSS Mushab, DY Park and D Choi. Synergistic effect of hydroxyapatite-magnetite nanocomposites in magnetic hyperthermia for bone cancer treatment. *Nanotechnology Reviews* 2024; **13(1)**, 20230225.

[40] N Ohtsu, Y Kakuchi and T Ohtsuki. Antibacterial effect of zinc oxide/hydroxyapatite coatings prepared by chemical solution deposition. *Applied Surface Science* 2018; **445**, 596-600.

[41] K Sinulingga, M Sirait, N Siregara and H Abdullah. Synthesis and characterizations of

natural limestone-derived nano-hydroxyapatite (HAp): A comparison study of different metals doped HAps on antibacterial activity. *RSC Advances* 2021; **11(26)**, 15896-15904.

[42] DAC Ferreira-Ermita, FL Valente, EC Carlo-Reis, FR Araújo, IM Ribeiro, CCV Cintra and APB Borges. Characterization and *in vivo* biocompatibility analysis of synthetic hydroxyapatite compounds associated with magnetite nanoparticles for a drug delivery system in osteomyelitis treatment. *Results in Materials* 2020; **5**, 100063.

[43] A Nikmah and R Kurniawan. Sintesis Hydroxyapatite Nanoparticle dari Limbah Cangkang Bekicot dan Aktivitas Antibakterinya sebagai Kandidat Material Biomedis. *Jurnal Sains dan Edukasi Sains* 2024; **7(1)**, 23-28.

[44] Charlena, IH Suparto and E Kurniawan. Synthesis and characterization of Hydroxyapatite-Zinc Oxide (HAp-ZnO) as antibacterial biomaterial. *IOP Conference Series: Materials Science and Engineering* 2018; **599**, 012011.

[45] M Hassanain, HM Abdel-Ghafar, HI Hamouda, FI El-Hosiny and EMM Ewais. Enhanced antimicrobial efficacy of hydroxyapatite-based composites for healthcare applications. *Scientific Reports* 2024; **14(1)**, 26426.